Journal of Sound and Vibration 329 (2010) 2616–2634

Contents lists available at ScienceDirect

Journal of Sound and Vibration

journal homepage: www.elsevier.com/locate/jsvi

Estimation of interfacial forces in time domain for linear systems

Aydin Gunduz, Akira Inoue, Rajendra Singh *

Acoustics and Dynamics Laboratory, Smart Vehicle Concepts Center, Department of Mechanical Engineering, The Ohio State University, Columbus, OH 43210, USA

ARTICLE INFO

Article history:
Received 21 April 2009
Received in revised form
28 December 2009
Accepted 2 January 2010
Handling Editor: K. Shin
Available online 11 February 2010

ABSTRACT

A structural path rank ordering process under transient excitations requires a good knowledge of the interfacial path forces, which are difficult to directly measure. Four time domain methods to estimate the interfacial forces are proposed and comparatively evaluated with application to linear time-invariant, proportionally damped discrete systems. First, the transient response is derived by modal analysis and a direct time domain technique to calculate the interfacial forces is outlined. Next, the frequency domain estimation methods, based on the sub-system concept are reviewed, and an inverse Fourier transform scheme is introduced. An indirect method of estimating interfacial force in transient state is then developed through an inverse procedure of modal analysis. The sub-system approach is employed to obtain the interfacial forces based on the forced vibration response of the original system and modal data of the sub-system. Finally, an approximate time domain scheme is suggested that could be used only if the system properties are known or precisely estimated. Although the proposed indirect methods are designed for eventual experimental applications, this article provides numerical feasibility studies via a simple source–path–receiver system (with parallel vibration paths) that has five translational degrees of freedom. The proposed methods are compared under ideal impulse force excitation input and a periodic sawtooth load (without and with Gaussian noise) to observe the starting transients as well as subsequent motions and interfacial forces. Preliminary comparisons with a laboratory experiment are very promising.

1. Introduction

The knowledge of dynamic forces at sub-system interfaces or attachments is of interest from both scientific and practical perspectives [1–4]. The nature of in situ interfacial forces can be illustrated by a generic vibration problem of Fig. 1, which conceptually describes many real-life problems where multiple vibration transmission paths exist [4–6]. Here a vibration source transmits dynamic forces and motions to the receiver through three parallel structural paths; the receiver is assumed to be disconnected from other structures. In our system, interfacial forces are denoted by $q_{ij}(t)$ in time (t) domain or by $\tilde{Q}_{ij}(\omega)$ in frequency (ω) domain, where the subscripts i and j refer to the adjoining sub-systems i and j. In most practical cases, installation of the dynamic force transducer(s) is impractical (or very difficult). Moreover, a force transducer would alter the interfacial conditions anyway unless there is significant mobility mismatch over a particular frequency regime [7]. Therefore, indirect methods are necessary to estimate the interfacial forces. It is the chief goal of this article with focus on time domain forces $q_{ij}(t)$.

* Corresponding author. Tel.: +1 614 292 9044; fax: +1 614 292 3163.
E-mail address: singh.3@osu.edu (R. Singh).

0022-460X/$ - see front matter © 2010 Elsevier Ltd. All rights reserved.
doi:10.1016/j.jsv.2010.01.003

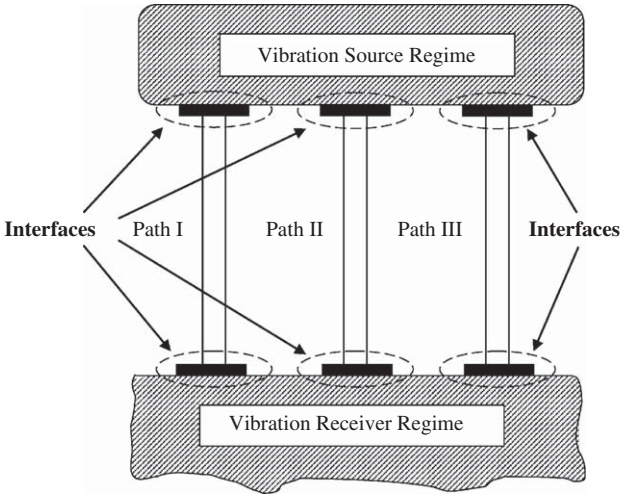

Fig. 1. Illustration of interfaces in a vibration problem with multiple transmission paths.

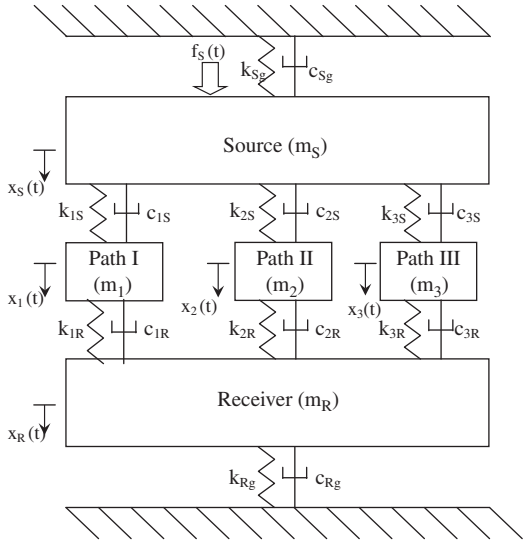

Fig. 2. Example case 5-DOF mechanical system depicting three parallel paths, single source and single receiver. Like Fig. 1, each path is assumed to possess mass only and all interfaces are described by linear springs and viscous damping elements.

For the sake of simplicity, assume that in situ interfaces can be described by linear, stiffness k_{ij} and viscous damping c_{ij} terms as illustrated in Fig. 2, which represents a discrete representation of Fig. 1. The interfacial forces can be directly calculated by the following:

$$q_{ij}(t) = -k_{ij}(x_i(t) - x_j(t)) - c_{ij}(\dot{x}_i(t) - \dot{x}_j(t)) \tag{1a}$$

$$\tilde{Q}_{ij}(\omega) = -(k_{ij} + \mathrm{j}\omega c_{ij})(\tilde{X}_i(\omega) - \tilde{X}_j(\omega)) \tag{1b}$$

where $q_{ij}(t)$ and $\tilde{Q}_{ij}(\omega)$ are the interfacial forces in time and frequency domains, respectively. The tilde denotes a complex value ($\mathrm{j} = \sqrt{-1}$). The lower case symbols such as $x_i(t)$and $x_j(t)$ are the displacements in time domain of the adjoining inertial elements; upper case symbols ($\tilde{X}_i(\omega), \tilde{X}_j(\omega)$) are complex-valued displacements in frequency domain and dots above the displacements represent time derivatives. Note that the relative motions of the adjoining structures and in-situ interfacial properties must be precisely known if Eq. (1a) were to be experimentally or computationally implemented (assuming a linear system of course). Now consider when the contact (interfacial) condition is very hard (i.e. k_{ij} is very high), the case where the estimated force could contain significant errors due to difficulties in measuring relative responses ($x_i(t) - x_j(t), \dot{x}_i(t) - \dot{x}_j(t)$). Very small differences in the displacements could induce a large error in the force. Further, in-situ stiffness and damping values are often unknown and thus implementation of Eq. (1a) is rather elusive in practical systems.

There is a significant body of literature on the frequency domain based transfer path analysis methods [1–6,8–12], where the interfacial forces are implicitly or explicitly estimated. For instance, several indirect frequency domain formulations have been established to estimate interfacial forces or moments in discrete systems [1–4]. These employ frequency response functions (FRFs) of the subsequent sub-system only at the driving points, assuming that the six-dimensional motions are somehow known (or measurable) at any location [1]. Experimental measurement burden could be significantly reduced provided that the interfacial forces are estimated only from the forced responses and FRFs at the driving point.

Although the transfer path analysis technique is well studied in the frequency domain, very few attempts have been made to formulate it for transient states in time domain [13]. A major difficulty in time domain is related to the convolution product whereas it corresponds to a simple product in frequency domain. Earlier time domain studies mostly focused on modal testing and parameter identification techniques [14–17]. Some recent studies have proposed system identification schemes in time domain that estimate stiffness and damping properties using measured accelerations [18–20]. A few researchers have also analyzed the deconvolution problem to indirectly estimate the unknown force excitations given the transient response data [21–25]. Transfer function based methods have been suggested to solve the inverse problem with an emphasis on the Tikhonov and truncated singular value decomposition regularization to overcome the ill-conditioned nature of the inverse problem. The L-curve and generalized cross-validation methods have been utilized to select the optimal regularization parameter. Yet, other approaches, such as the sum of weighted accelerations technique, and inverse filtering, have been proposed to solve the inverse problem [26–28]. The above mentioned force reconstruction methods, however, concentrate on the estimation of input force(s) and not on the constraint or interfacial forces. This paper outlines several methods to estimate the transient interfacial forces and proposes an alternative time domain approach to solve the inverse problem with an emphasis on interfacial forces.

2. Problem formulation

2.1. Scope and objectives

Consider a linear, time-invariant mechanical or structural system consisting of mass **M**, proportional viscous damping **C** and stiffness **K** matrices of dimension N (bold symbols indicate matrices or vectors):

$$\mathbf{M}\ddot{\mathbf{x}}(t)+\mathbf{C}\dot{\mathbf{x}}(t)+\mathbf{K}\mathbf{x}(t)=\mathbf{f}(t) \tag{2}$$

where $\mathbf{f}(t)$ is the external force vector and $\mathbf{x}(t)$ is the displacement response vector. Knowing the system response $\mathbf{x}(t)$ to either harmonic or transient excitation, interfacial forces ($q_{ij}(t)$) could be indirectly estimated by utilizing the sub-system approach [1], which is based on the premise that the interfacial forces of a system are equivalent to the external forces acting on its sub-systems that are subsequent (downward) from the interfacial connections.

The force calculation methods in frequency domain estimate time-averaged solutions that correspond to the steady state responses in time domain [29,30]. For a linear time-invariant system with sufficient damping, the steady-state would be reached within a short time, and the time-averaged values (in frequency domain) could give the primary solution. However, when the system is lightly damped or being excited by a pure transient excitation, a time domain analysis is desirable and particularly useful from the application perspective, including the dynamic design of attachments and connection elements. For instance, an engine start-up, rotating machinery shut-down, impacts generated due to clearances (such as in gears) or an intermittent operation of an electro-mechanical actuator are some practical examples where significant transient or impulse-like forces are observed. Accordingly we establish the following objectives of this paper: 1. Formulate an indirect interfacial force estimation method under the transient state for a proportionally damped discrete system with arbitrary excitation using the inverse modal analysis. 2. Conduct feasibility studies of this method by comparing it with the direct time domain solution and the inverse frequency domain approach. 3. Conduct a laboratory experiment corresponding to Fig. 1 and validate the proposed method on a preliminary basis.

One difficulty in the direct or indirect force estimation method (in time domain) is related to the numerical evaluation of the convolution integral. We overcome this difficulty by assuming that the system is properly discretized by choosing representative response points. The evaluation (measurement) time is also discretized and this would transform the convolution integral into a summation over the relevant duration. Further, in order to formulate an indirect interfacial force estimation method based on the inverse modal analysis procedure, eigensolutions of the downward sub-system could be utilized in the formulation. The convolution integral (or a summation) must be inversely solved with a regression algorithm about the generalized force in modal domain.

2.2. Example case: 5-DOF source–path–receiver network with 6 interfaces

The example case for computational studies is a 5 degrees of freedom (DOF), source–path–receiver model (as shown in Fig. 2) although other source–path–receiver combinations can be analyzed as well [31,32]. This model captures the essence of the generic interface problem of Fig. 1. Here, the system consists of single degree of freedom source (subscript S) and receiver (subscript R) regimes. The interfaces are described by Voight-type viscoelastic elements (with in-situ stiffness and

Table 1
Parameters and modal properties of the example case of Fig. 2. (a) System parameters. (b) Natural frequencies, orthonormalized eigenvectors and modal damping ratios.

(a)						
Mass elements m (kg)				m_S=1.48, m_R=2.48, m_1=0.50, m_2=0.90, m_3=0.70		
Stiffness elements k (kN/m)				k_{1S}=k_{1R}=70, k_{2S}=k_{2R}=50, k_{3S}=k_{3R}=40, k_{Rg}=90, k_{Sg}=0		
Damping elements c (Ns/m)				c_{1S}=c_{1R}=14, c_{2S}=c_{2R}=10, c_{3S}=c_{3R}=8, c_{Rg}=90, c_{Sg}=0		
Proportionality constant α (s)				0.0002		
(b)						
Mode index r		1	2	3	4	5
Natural frequency Ω_r (Hz)		5.60	15.3	23.4	28.1	33.1
Modal vectors $\mathbf{u}_r$	X_S	0.1629	−0.1334	0.0366	−0.0318	−0.0575
	X_1	0.1361	0.0173	0.0801	−0.1507	0.4794
	X_2	0.1404	0.0245	−0.4180	0.0533	0.0458
	X_3	0.1375	0.0192	0.1322	0.5658	0.1161
	X_R	0.1006	0.1599	0.0342	−0.0278	−0.0488
Modal damping ratios ζ_r		0.0035	0.0096	0.0147	0.0177	0.0208

damping); each interface is given by complex-valued stiffness $\tilde{k}_{ij} = k_{ij} + j\omega c_{ij}$ at frequency ω. Paths between the interfaces are assumed to be rigid and given by masses (m_1,m_2,m_3). Refer to Fig. 2 for all symbols. All stiffness elements are represented as a combination of an ideal spring and an associated ideal (viscous) damper with a proportionality constant α (i.e. $c_{ij} = \alpha k_{ij}$ or $\mathbf{C} = \alpha\mathbf{K}$). In time domain, the force excitation within the source regime is denoted by $f_S(t)$ and the resulting displacement of each mass is designated as $x_i(t)$ (i=S,1,2,3,R). Only vertical motions are considered. The structural properties of this example are listed in Table 1(a).

For a proportionally damped system of dimension N, $\mathbf{Ku} = \Omega^2\mathbf{Mu}$ is solved to obtain undamped natural frequencies Ω_r and generalized eigenvectors $\mathbf{u}_r$ ($r = 1, \ldots, N$) where r is the modal index. The normal mode matrix $\mathbf{U} = [\mathbf{u}_1, \ldots, \mathbf{u}_N]_{N\times N}$ is orthonormalized as $\mathbf{U^T MU} = \mathbf{I}$, $\mathbf{U^T KU} = \mathrm{diag}[\Omega_r^2]$ and $\mathbf{U^T CU} = \mathrm{diag}[2\zeta_r\Omega_r]$, where $\mathbf{I}$ is the identity matrix, diag indicates a diagonal matrix and ζ_r are the modal damping ratios. See Table 1(b) for the eigenvalues $\mathbf{f}(t)$, orthonormalized eigenvectors ($\mathbf{u}_r$) and ζ_r values for the 5-DOF system. System parameters of Table 1(a) are adjusted such that the natural frequencies are separated by at least 5 Hz. The dynamic compliance magnitude spectra $|\tilde{X}_i/F_S(\omega)|$ ($i = 1, 2, 3, \mathrm{R}$) are plotted in Fig. 3. Sharp peaks at the resonances show that the system is lightly damped as also evident from the low damping ratios reported in Table 1(b). The highest peak among the five resonances is at the first natural frequency, 5.6 Hz, where all masses participate. The second highest peak of the receiver is at the second natural frequency, 15.3 Hz, but this peak is not very significant for the paths. However, paths 2, 1 and 3 are most excited, respectively, at 23.4, 28.1 and 33.1 Hz.

Figs. 4(a) and (b) show the relevant 4-DOF sub-systems that would be utilized to estimate the interfacial forces on the source side ($q_{iS}(t)$, $i = 1, 2, 3$), and on the receiver side ($q_{iR}(t)$, $i = 1, 2, 3$), respectively, by the sub-system methods discussed in Sections 4–6. The same sub-systems are selected for either time or frequency domain methods. Any method that utilizes the sub-system approach (thus a force reconstruction) will be considered as an indirect method in the paper. Conversely, the force estimation from relative response calculations (by Eq. (1a–b) as discussed in the next section) will be considered as a direct method as this formulation does not require a sub-system concept to indirectly reconstruct the forces from absolute response measurements.

3. Transient response and estimation of interfacial forces by a direct time domain method (Method A)

For a proportionally damped system, the time domain response is expressed as a superposition of the normal modes since the modal matrix $\mathbf{U}$ decouples the equations of motion:

$$\mathbf{x}(t) = \mathbf{U}\boldsymbol{\chi}(t) \tag{3}$$

Here, $\boldsymbol{\chi}(t)$ is the generalized coordinate (displacement). The external force in modal domain is also transformed as $\mathbf{U}^T\mathbf{f}(t) = \boldsymbol{\Lambda}(t)$. For the rth mode $\chi_r(t) = \chi_r^{\mathrm{CI}}(t) + \chi_r^{\mathrm{initial}}(t)$ is expressed by the convolution integral plus initial condition terms (refer to Appendix A.1. for an analytical derivation):

$$\chi_r(t) = \frac{1}{\Omega_{rd}}\int_0^t \Lambda_r(\tau)\mathrm{e}^{-\zeta_r\Omega_r(t-\tau)}\sin\{\Omega_{rd}(t-\tau)\}\,\mathrm{d}\tau + A_1(t)\chi_r(0) + A_2(t)\dot{\chi}_r(0) \tag{4a}$$

$$A_1(t) = \mathrm{e}^{-\zeta_r\Omega_r t}\left(\cos\Omega_{rd}t + \frac{\zeta_r}{\sqrt{1-\zeta_r^2}}\sin\Omega_{rd}t\right); \quad A_2(t) = \frac{1}{\Omega_{rd}}\mathrm{e}^{-\zeta_r\Omega_r t}\sin\Omega_{rd}t \tag{4b-c}$$

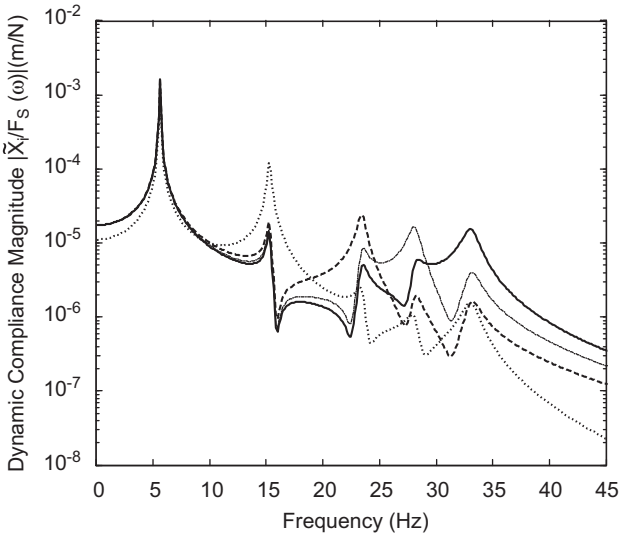

Fig. 3. Dynamic compliance magnitude spectra at paths (1, 2, 3) and receiver (R) given uniform excitation $\tilde{F}_S(\omega)$ at the source. Key: (———) $|\tilde{X}_1/F_S(\omega)|$; (- - - - -) $|\tilde{X}_2/F_S(\omega)|$; (-·-·-·-·-) $|\tilde{X}_3/F_S(\omega)|$; and (·····) $|\tilde{X}_R/F_S(\omega)|$.

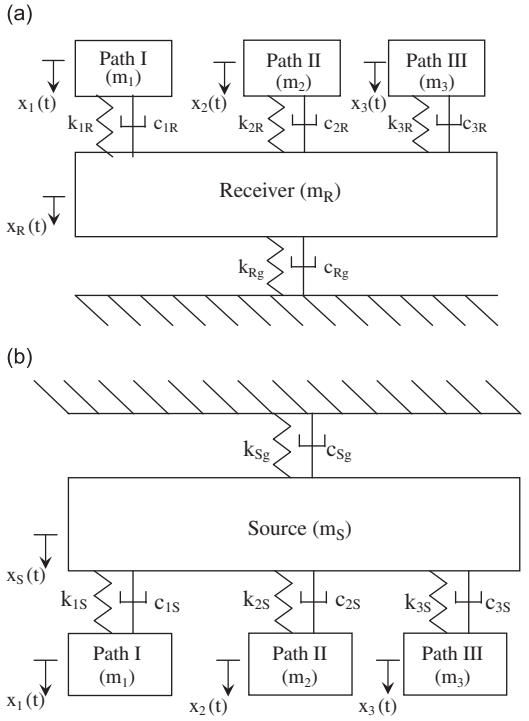

Fig. 4. Sub-systems utilized for indirect interfacial force estimation methods: (a) sub-system to determine the interfacial forces $q_{iS}(t)$ and $\tilde{Q}_{iS}(\omega)$ on the source (S) side and (b) sub-system to determine the forces $q_{iR}(t)$ and $\tilde{Q}_{iR}(\omega)$ on the receiver (R) side.

Then, the transient response is given by Eqs. (3) and (4a). If both the interfacial properties (k_{ij} and c_{ij}) and the transient motion response are known, the interfacial forces can be estimated by the direct method as given by Eq. (1a), where the differentiation (or integration) may numerically be executed as

$$\dot{x}(t_i) \approx \frac{x(t_{i+1})-x(t_i)}{t_{i+1}-t_i}; \quad x(t_i) = \int_{t_i}^{t_{i+1}} \dot{x}(t_i)\,\mathrm{d}t \approx \frac{1}{2}(t_{i+1}-t_i)(\dot{x}(t_{i+1})+\dot{x}(t_i)) \tag{5a-b}$$

We designate this calculation technique as "Method A" and consider it as a direct method as mentioned in Section 2.

For discrete time events or measured data the evaluation (measurement) time is discretized as $t = t_1, t_2, \ldots, t_d$ (s) such that $t_1 = 0$ and time resolution $h = t_{i+1} - t_i$. For subsequent use, the convolution integral (Eq. (4a)) is now approximated by a summation that may be obtained by calculating each trapezoid area between each time interval. At $t = t_d = (d-1)h$, the integrand χ_r^{CI} in Eq. (4a) takes d values and the convolution integral may be calculated by a sum of $(d-2)$ trapezoid areas and one triangle area as described below (Appendix A.2. provides an analytical derivation):

$$\tau = 0 : \Lambda_r(0)\mathrm{e}^{-(d-1)\zeta_r\Omega_r h}\sin(d-1)\Omega_{rd}h \equiv I_{d-1}^{(0)} \tag{6a}$$

$$\tau = h : \Lambda_r(h)\mathrm{e}^{-(d-2)\zeta_r\Omega_r h}\sin(d-2)\Omega_{rd}h \equiv I_{d-1}^{(h)} \tag{6b}$$

$$\tau = 2h : \Lambda_r(2h)\mathrm{e}^{-(d-3)\zeta_r\Omega_r h}\sin(d-3)\Omega_{rd}h \equiv I_{d-1}^{(2h)} \tag{6c}$$

$$\vdots$$

$$\tau = jh : \Lambda_r(jh)\mathrm{e}^{-(d-1-j)\zeta_r\Omega_r h}\sin(d-1-j)\Omega_{rd}h \equiv I_{d-1}^{(jh)} \tag{6d}$$

$$\vdots$$

$$\tau = (d-1)h : \Lambda_r((d-1)h)\mathrm{e}^{0}\sin 0 = 0 \tag{6e}$$

Therefore, the convolution integral in $\chi_r^{\mathrm{CI}}(t)$ is estimated by

$$\chi_r^{\mathrm{CI}}(t_d) = \chi_r((d-1)h) = \frac{h}{\Omega_{rd}}\sum_{j=1}^{d-2} I_{d-1}^{(jh)} + \frac{h}{2\Omega_{rd}} I_{d-1}^{(0)} \tag{7}$$

Note that the difference in the integrand I depends on the end time of each interval. Also, observe that the convolution integral term $\chi_r^{\mathrm{CI}}(t)$ does not include the initial conditions at $t = t_1 = 0$. When the initial conditions ($\mathbf{x}_0$ and $\dot{\mathbf{x}}_0$) are known (or applicable), the initial term $\chi_r^{\mathrm{initial}}(t)$ in Eq. (4a) is easily estimated.

4. Frequency domain methods and inverse fast Fourier transform (Method B)

4.1. Estimation of interfacial forces in frequency domain

Interfacial forces are next indirectly estimated in frequency domain based on the forced harmonic responses of the system and frequency response functions (FRFs) of sub-systems that are downward from the interfacial points. Note that even though an indirect, yet exact, formulation can be developed for analytical or computational work, some difficulties arise in implementing it in practice due to measurement restrictions [1].

Consider a harmonic excitation force $f_i(t)$ at any mass m_i in Fig. 2. Under steady state, forces and resulting displacement responses are

$$\begin{cases} f_i(t) = F_i\cos(\omega t + \varphi_{f_i}) = \mathrm{Re}[\tilde{F}_i\mathrm{e}^{\mathrm{j}\omega t}] \\ x_i(t) = X_i\cos(\omega t + \varphi_{x_i}) = \mathrm{Re}[\tilde{X}_i\mathrm{e}^{\mathrm{j}\omega t}] \end{cases} \tag{8a, b}$$

The complex-valued amplitudes $\tilde{F}_i(=F_i\mathrm{e}^{\mathrm{j}\varphi_{f_i}})$ and $\tilde{X}_i(=X_i\mathrm{e}^{\mathrm{j}\varphi_{x_i}})$ include phases (φ_{f_i},φ_{x_i}). The ubiquitous $\mathrm{e}^{\mathrm{j}\omega t}$ terms are omitted henceforth. The governing equations at ω corresponding to Eq. (2) are

$$[\tilde{\mathbf{K}}(\omega) - \omega^2\mathbf{M}]\tilde{\mathbf{X}}(\omega) = \tilde{\mathbf{F}}(\omega) \tag{9}$$

where $\tilde{\mathbf{K}}$ is the complex stiffness $\tilde{\mathbf{K}}(\omega) = \mathbf{K} + \mathrm{j}\omega\mathbf{C}$, $\tilde{\mathbf{X}}(\omega) = (\tilde{X}_1, \ldots, \tilde{X}_N)^{\mathrm{T}}$ and $\tilde{\mathbf{F}}(\omega) = (\tilde{F}_1, \ldots, \tilde{F}_N)^{\mathrm{T}}$. If necessary, structural damping could be described as $\tilde{\mathbf{K}}' = \mathbf{K} + \mathrm{j}\mathbf{C}_{\mathrm{structural}}$. The displacement responses of Eq. (9) may be solved either by matrix inversion or by modal analysis:

$$\tilde{\mathbf{X}}(\omega) = \tilde{\mathbf{Z}}^{-1}(\omega)\tilde{\mathbf{F}}(\omega) = \tilde{\mathbf{H}}(\omega)\tilde{\mathbf{F}}(\omega), \quad \text{where} \quad \tilde{\mathbf{Z}}(\omega) = \tilde{\mathbf{H}}^{-1}(\omega) = \tilde{\mathbf{K}}(\omega) - \omega^2\mathbf{M} \tag{10}$$

$$\tilde{\mathbf{X}}(\omega) = \sum_{r=1}^{N} \frac{\mathbf{u}_r^{\mathrm{T}}\tilde{\mathbf{F}}(\omega)}{\Omega_r^2 - \omega^2 + 2\mathrm{j}\omega\zeta_r\Omega_r}\mathbf{u}_r \tag{11}$$

Eq. (10) could be used for either proportional or non-proportionally damped systems, but the matrix inversion process could involve computational issues, such as ill-conditioning (singularity) and intense calculation time. Thus, Eq. (11) is often preferred for proportionally damped systems. Since a periodic input can be decomposed into a sum of harmonic terms by Fourier series, Eqs. (10) and (11) are valid for periodic excitations as well.

The interfacial forces can be indirectly estimated using the sub-system concept. Define the dynamic compliances $\tilde{H}_{u,v} = (\tilde{X}_u/F_v(\omega))$ of the sub-system, where $u, v = 1, \ldots, g$. Here g is the dimension of the sub-system. Interfacial forces can

be determined at each ω by inverting $\tilde{\mathbf{H}}(\omega)$ of the sub-system, together with the forced vibrations of the whole system:

$$\begin{pmatrix} \tilde{F}_1(\omega) \\ \vdots \\ \tilde{F}_g(\omega) \end{pmatrix} = \begin{pmatrix} \tilde{H}_{1,1}(\omega) & \cdots & \tilde{H}_{1,g}(\omega) \\ \vdots & & \vdots \\ \tilde{H}_{g,1}(\omega) & \cdots & \tilde{H}_{g,g}(\omega) \end{pmatrix}^{-1}_{\text{sub-system}} \begin{pmatrix} \tilde{X}_1(\omega) \\ \vdots \\ \tilde{X}_g(\omega) \end{pmatrix}_{\substack{\text{whole} \\ \text{system}}} \tag{12}$$

where $\tilde{F}_u(\omega)(u=1,\ldots,g)$ are equivalent to the interfacial forces $\tilde{Q}_{ij}(\omega)$ of the original system. Expanding Eq. (12) for the uth path and decomposing it into contributions from each path, interfacial forces for the uth path can also be found as

$$\tilde{Q}_{ij}(\omega) = \tilde{F}_u(\omega) = \sum_n \frac{\tilde{F}_u}{\tilde{X}_n}(\omega)\bigg|_{\text{BBC}} \tilde{X}_n(\omega) \tag{13}$$

where the summation about n is taken for the interfacial points and $\tilde{F}_u/X_n(\omega)$ are the dynamic stiffness terms of the sub-system with blocked boundary conditions (BBCs) [1,33,34]. The main advantage of Eq. (13) over Eq. (12) is that only driving-point FRFs are required by Eq. (13) when determining the interfacial forces. However, it is difficult to implement the blocked boundary conditions in experimental work. Hence, the matrix inversion method Eq. (12) is often employed although it requires additional calculations or measurements.

Alternatively, the pseudo-inverse method (given by superscript +) may also be used to determine the interfacial forces [23–25]:

$$\tilde{\mathbf{F}}(\omega) = (\tilde{\mathbf{H}}(\omega))^+ \tilde{\mathbf{X}}(\omega)$$

$$(\tilde{\mathbf{H}}(\omega))^+ = [(\tilde{\mathbf{H}}(\omega))^{\mathrm{T}}(\tilde{\mathbf{H}}(\omega))]^{-1}(\tilde{\mathbf{H}}(\omega))^{\mathrm{T}} \tag{14a, b}$$

Observe that the indirect formulations (Eqs. (12)–(14)) are exact and equivalent to the direct formulation (Eq. (1b)). Refer to [1] for analytical details and some closed form solutions.

4.2. Estimation of interfacial forces by inverse Fourier transform (Method B)

One common practice to obtain the time domain response of a vibratory system is to employ the inverse fast Fourier transform (IFFT) given the frequency domain results [35]. For discrete-time data, sequence $y(nh)$ in time domain is given by

$$y(nh) = \Delta f \sum_{k=0}^{N_p-1} \tilde{Y}(k\,\Delta f)\mathrm{e}^{\mathrm{j}(2\pi kn/N_p)}, \quad n = 0,1,2,\ldots,N_p-1 \tag{15}$$

where n is the sequence index, h the time resolution (s), Δf the frequency resolution (Hz), N_p the number of points and k the spectral index. The corresponding fast Fourier transform (FFT) is defined as follows:

$$\tilde{Y}(k\,\Delta f) = h \sum_{k=0}^{N_p-1} y(nh)\mathrm{e}^{-\mathrm{j}(2\pi kn/N_p)}, \quad k = 0,1,2,\ldots,N_p-1 \tag{16}$$

Now, consider an ideal periodic sawtooth input $f_S(t)$ with a period of $T=0.1$ s, and amplitude of $A=10$ N, as shown in Fig. 5(a). The spectral content of this input $|\tilde{F}_S(\omega)|$ is shown in Fig. 6(a), and the resulting displacement response spectra for the paths and the receiver $|\tilde{X}_i(\omega)|$ (i=1,2,3,R) are displayed in Fig. 6(b). The receiver response ($x_R(t)$) and the interfacial forces on the source side of path 1 ($q_{1S}(t)$) are calculated by two alternate methods: (i) find the "true" transient response by Eq. (4a) and employ Method A; (ii) employ Eq. (15) given $\tilde{Q}_{1S}(\omega)$ obtained by using Eq. (12) with a selected sampling frequency $f_{sp}=500$ Hz, and number of data points $N_p=4096$ (2^{12}). Figs. 5(b) and (c) show that the second method disregards the majority of the starting transients for the selected time window ($t_{sp}=8.192$ s). If the sawtooth amplitude A is increased, the starting transients would be even more significant. Obviously such transients cannot be disregarded. To improve the IFFT based force estimate (for a given external excitation), we suggest one of the following two strategies.

Strategy I. Increase the number of data points (say $2^{14}=16{,}384$ points for the example case) to extend t_{sp} and sample a longer transient duration. The number of needed points however would increase even more (theoretically to infinity) for systems with small damping and for transient excitations such as an impulse-like excitation.

Strategy II. First, calculate the "true" transient $\mathbf{x}(t)$ using Eq. (4a). Second, transform the response to frequency domain ($\tilde{\mathbf{X}}(\omega)$) by FFT (Eq. (16)). Third, calculate the interfacial forces in frequency domain by Eq. (12). Finally, transform the interfacial forces back to the time domain by the IFFT process (Eq. (15)) and obtain transient $q_{ij}(t)$. We designate this calculation strategy as Method B.

Although accurate results with a lower N_p may be obtained by the second strategy (Method B), the overall accuracy still depends on a proper selection of the sampling parameters. For example the sampling frequency (f_{sp}) should be at least four times greater than the maximum analysis frequency to avoid the aliasing problem and yet Δf should be kept small enough to capture the details in the spectrum. A typical error analysis is given in Table 2, where the average root-mean-square

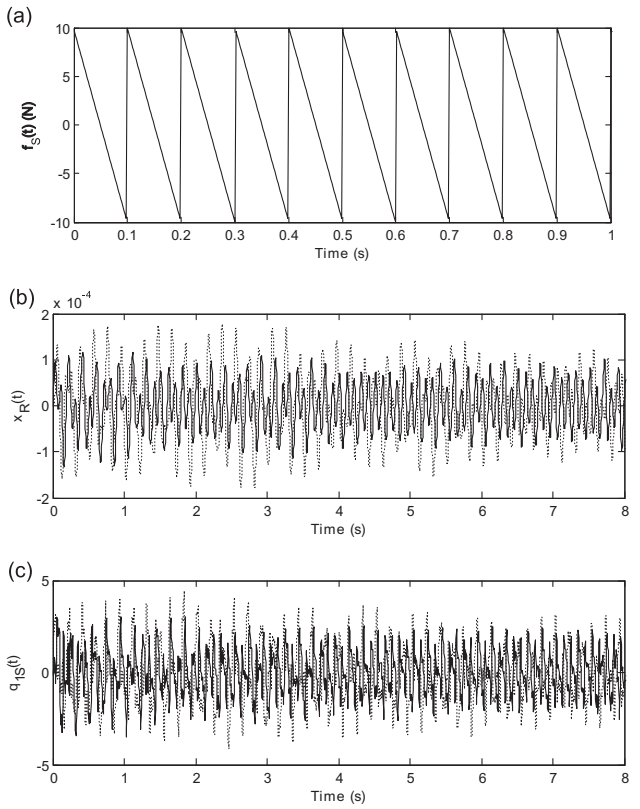

Fig. 5. Sawtooth excitation and responses in time domain: (a) periodic sawtooth force with T=0.1 s and A=10 N; (b) resulting $x_R(t)$ and (c) resulting $q_{1S}(t)$. Key: (·····), time domain method (method B) and (———), frequency domain (steady state) method.

errors (ε_{rms}) in transient forces, as yielded by Method B, are shown for various f_{sp} assuming that Method A yields the true solution for an ideal input (which is validated later in Section 7):

$$\varepsilon_{\text{rms}} = \frac{1}{N_p}\sqrt{\sum_{n=1}^{N_p}(q_{ij}(t) - q_{ij}^{\text{ideal}}(t))^2} \tag{17}$$

When the sampling frequency f_{sp} is reduced, a rapid growth in errors is seen in Table 2. Since we are primarily interested in lower frequency regime and the Ω_r values of the example case are between 5.6 and 33.1 Hz, a relatively low f_{sp} (such as 500 Hz) yields satisfactory results. However, when the system has higher natural frequencies, a very high value of f_{sp} should be chosen; this would significantly reduce the time window (t_{sp}) for a given N_p (and that would yield additional sampling errors). Hence, selection of sampling parameters is a primary issue whenever Method B were to be employed. Also, one should apply proper windows to avoid the leakage problem and to ensure that no transients are "edited" out. Given the underlying sampling issues and two domain transformations (using the computational process), true time domain approaches, as described next in Sections 5 and 6, propose promising alternatives to the IFFT method to estimate the transient interfacial forces.

5. Indirect interfacial force estimation in time domain by inverse modal analysis (Method C)

Recall the matrix formulation that was developed in Section 4 (Eq. (12)) to determine the interfacial forces in frequency domain utilizing the forced (whole) system response ($\tilde{\mathbf{X}}(\omega)$), and the dynamic compliance matrix ($\tilde{\mathbf{H}}(\omega)$) of the sub-system. The corresponding time domain formulation can be expressed in the following convolution ($*$) product:

$$\begin{pmatrix} f_1(t) \\ \vdots \\ f_g(t) \end{pmatrix}_{\substack{\text{whole} \\ \text{system}}} = \begin{pmatrix} h_{1,1}(t) & \cdots & h_{1,g}(t) \\ \vdots & & \vdots \\ h_{g,1}(t) & \cdots & h_{g,g}(t) \end{pmatrix}^{-1}_{\text{sub-system}} * \begin{pmatrix} x_1(t) \\ \vdots \\ x_g(t) \end{pmatrix}_{\substack{\text{whole} \\ \text{system}}} \tag{18}$$

Here $h_{i,j}(t)$ are the impulse response terms of the sub-system, and $f_u(t)(u=1,\cdots,g)$ are equivalent to the interfacial forces $q_{ij}(t)$ of the original (whole) system. However, this calculation approach is extremely inefficient as it requires g^2

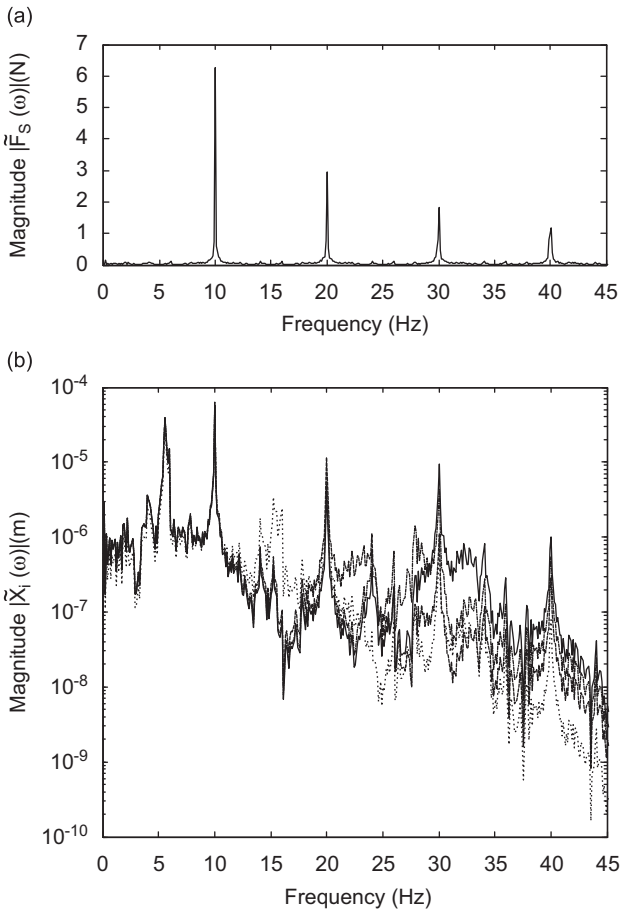

Fig. 6. Sawtooth force and responses in frequency domain: (a) force spectrum (FFT of Fig. 5(a)) and (b) displacement response magnitude spectra at paths (1, 2, 3) and receiver. Key: (———) $|\tilde{X}_1(\omega)|$; (- - - - -) $|\tilde{X}_2(\omega)|$; (-·-·-·-·-) $|\tilde{X}_3(\omega)|$; (••••••••••) $|\tilde{X}_R(\omega)|$.

Table 2
Average root-mean-square errors (ε_{rms}) as caused by the choice of sampling frequency (f_{sp}) in Method B. Benchmark is the true response yielded by Method A.

	ε_{rms} in interfacial force (N)			
Interfacial force	f_{sp}=1000 Hz	f_{sp}=500 Hz	f_{sp}=300 Hz	f_{sp}=100 Hz
q_{1S}(t)	0.0004	0.0007	0.0065	0.0202
q_{2S}(t)	0.0003	0.0005	0.0046	0.0146
q_{3S}(t)	0.0002	0.0004	0.0037	0.0116
q_{1R}(t)	0.0024	0.0047	0.0069	0.0126
q_{2R}(t)	0.0017	0.0034	0.0049	0.0091
q_{3R}(t)	0.0016	0.0027	0.0040	0.0072

convolution integral calculations at each discrete time, which is practically impossible to execute. The time domain correspondents of Eqs. (13) and (14) also have the same problem. Therefore, the regression algorithm illustrated in Section 3 (and derived in Appendix A.2.) is utilized to develop a more tractable transient interfacial force estimation method.

Based on the response $\mathbf{x}(t)$ and modal data (Ω_r, ζ_r and $\mathbf{u}_r$), the external force $\mathbf{f}(t)$ to the system is constructed by an inverse procedure. In order to obtain the interfacial forces, utilize Ω_r, ζ_r and $\mathbf{u}_r$ of the sub-system whose external forces act as the interfacial forces, and $\mathbf{x}(t)$ of the whole system. Here, assume that $\mathbf{x}_0$ and $\dot{\mathbf{x}}_0$ are known. Because of the difference in the integrand I at each discrete time, the inverse modal synthesis is far more complicated than the regular modal analysis. The proposed steps are given below. (Refer to Appendix A.2. for equations starting with A.)

First, the response $\mathbf{x}(t)$ is transformed into modal domain by Eq. (11) applying $\mathbf{U}^{-1}\mathbf{x}(t)=\boldsymbol{\chi}(t)$. Then, the $\chi_r^{\mathrm{Cl}}(h)$ term is extracted as $\chi_r^{\mathrm{Cl}}(t)=\chi_r(t)-\chi_r^{\mathrm{initial}}(t)$, where $\chi_r^{\mathrm{initial}}(t)$ is known given $\mathbf{x}_0$ and $\dot{\mathbf{x}}_0$. When $t=t_2=h$, Eq. (A6) gives

$$\Lambda_r(0)=\frac{2\Omega_{rd}\chi_r^{\mathrm{Cl}}(h)}{h\Lambda_r^{\mathrm{den}}} \tag{19}$$

where $\Lambda_r(0)$ is the generalized force at $t=t_1=0$, and $\Lambda_r^{\mathrm{den}}\equiv \mathrm{e}^{-\zeta_r\Omega_r h}\sin\Omega_{rd}h$ is defined for the sake of convenience. Next, at $t=t_3=2h$, the generalized force at $t=t_2=h$ is obtained from Eq. (A8):

$$\Lambda_r(h)=\frac{\dfrac{\Omega_{rd}\chi_r^{\mathrm{Cl}}(2h)}{h}-\dfrac{I_2^{(0)}}{2}}{\Lambda_r^{Den}}=\frac{\dfrac{\Omega_{rd}\chi_r^{\mathrm{Cl}}(2h)}{h}-\dfrac{\Lambda_r(0)\mathrm{e}^{-2\zeta_r\Omega_r h}\sin 2\Omega_{rd}h}{2}}{\Lambda_r^{Den}} \tag{20}$$

where $\Lambda_r(0)$ is defined by Eq. (19). Next, at $t=t_4=3h$, the generalized force at $t=t_3=2h$ is obtained using Eq. (A10) as

$$\Lambda_r(2h)=\frac{\dfrac{\Omega_{rd}\chi_r^{\mathrm{Cl}}(3h)}{h}-\dfrac{I_3^{(0)}}{2}-I_3^{(h)}}{\Lambda_r^{\mathrm{Den}}} \tag{21a}$$

Replacing the integrands $I_3^{(0)}$ and $I_3^{(h)}$ of Eq. (21a) by Eqs. (A9a) and (A9b) gives

$$\Lambda_r(2h)=\frac{\dfrac{\Omega_{rd}\chi_r^{\mathrm{Cl}}(3h)}{h}-\dfrac{\Lambda_r(0)\mathrm{e}^{-3\zeta_r\Omega_r h}\sin 3\Omega_{rd}h}{2}-\Lambda_r(h)\mathrm{e}^{-2\zeta_r\Omega_r h}\sin 2\Omega_{rd}h}{\Lambda_r^{\mathrm{den}}} \tag{21b}$$

Here, $\Lambda_r(0)$ and $\Lambda_r(h)$ may be obtained from Eqs. (19) and (20), respectively.

Similarly, at $t=t_d=(d-1)h$, the generalized force at $t=t_{d-1}=(d-2)h$ is calculated using the previously obtained $\Lambda_r(jh)$ values for $j=1,\ldots,(d-3)$ as

$$\Lambda_r((d-2)h)=\frac{\dfrac{\Omega_{rd}\chi_r^{\mathrm{Cl}}((d-1)h)}{h}-\dfrac{I_{d-1}^{(0)}}{2}-\sum_{j=1}^{d-3}I_{d-1}^{(jh)}}{\Lambda_r^{\mathrm{den}}} \tag{22a}$$

Replacing the integrands of Eq. (22a) by Eqs. (6a) and (6d) gives

$$\Lambda_r((d-2)h)=\frac{1}{\Lambda_r^{\mathrm{den}}}\left[\frac{\Omega_{rd}\chi_r^{\mathrm{Cl}}((d-1)h)}{h}-\frac{\Lambda_r(0)\mathrm{e}^{-(d-1)\zeta_r\Omega_r h}\sin(d-1)\Omega_{rd}h}{2}-\sum_{j=1}^{d-3}\Lambda_r(jh)\mathrm{e}^{-(d-1-j)\zeta_r\Omega_r h}\sin(d-1-j)\Omega_{rd}h\right] \tag{22b}$$

Here, $\Lambda_r(0)$, $\Lambda_r(h),\ldots,\Lambda_r((\mathrm{d}-3)h)$ are the generalized forces at previous discrete time steps $t_1,t_2,\ldots,t_{\mathrm{d}-2}$ that are calculated during the execution of the regression algorithm. Unlike the response obtained in Section 3, which can be calculated in any order about time, the force obtained here (using the sub-system approach) must be calculated in the proper sequence at $t=t_1,t_2,\ldots,t_{d-1}$, from past to future, due to the regression algorithm about Λ_r. Note that the generalized force $\Lambda_r((\mathrm{d}-1)h)$ at $t=t_d=(d-1)h$ is still unknown, since the final terms, such as Eq. (6e), are always zero. Finally, the external force vector is estimated as

$$\mathbf{f}(t)=(\mathbf{U}^{\mathrm{T}})^{-1}\boldsymbol{\Lambda}(t) \tag{23}$$

Here, $t=t_1,t_2,\ldots,t_{d-1}$ due to the above mentioned limitation, and $\mathbf{f}(t_d)$ is still unknown. As noted before, $\mathbf{f}(t)$ of sub-system corresponds to $\mathbf{q}(t)$ of the original (whole) system. Note that although this reconstructed transient force vector $\mathbf{f}(t)$ has the same dimension as of the sub-system, the forces are, of course, zero at those elements, where no external force to the sub-system exists. For instance, if $q_{iS}(t)$ $(i=1,2,3)$ are of interest and sub-system of Fig. 4(a) is utilized, the forces on the receiver must be zero since there is no external force that acts on the receiver of the sub-system. The proposed estimation scheme developed in this section is labeled as "Method C". It should be a promising alternative to two methods (A and B) as well as to the other force reconstruction techniques that are well described in the literature [21–28].

6. Indirect interfacial force estimation in time domain using sub-system matrices (Method D)

The proposed estimation scheme of Section 5 (Method C) can be used only when the modal domain properties are fully known. However, if the system parameters ($\mathbf{M}$, $\mathbf{K}$ and $\mathbf{C}$) are known, interfacial forces can be estimated by a simpler, and approximate approach that is designated as Method D. In this formulation we simply incorporate the sub-system matrices in Eq. (2) along with corresponding measured responses, and execute the numerical differentiation or integration (Eq. (5)). Overall, Method D will have a somewhat limited utility for many practical problems since it is easier to measure relevant mode shapes and natural frequencies (as required by Method C) rather than estimating physical system properties. Although Methods A and D both require the knowledge of interfacial properties, the chief advantage of Method D over Method A is that it requires absolute motion measurements (instead of the relative motions), which is usually less erroneous and easier to measure in most real-life systems.

7. Comparative evaluation of four time domain methods (A–D)

The proposed transient methods are graphically summarized in Fig. 7. The left hand side of the schematic outlines the system response calculation given external excitation (for computational purposes), and the right hand side depicts the indirect interfacial force estimation methods. Note that the symbols f and f^{-1} stand for fast Fourier transform (FFT) and inverse fast Fourier transform (IFFT).

Next, the indirect force estimations (using Methods C and D) are computationally compared with the direct time domain calculation (Method A) and the frequency domain approach using IFFT (Method B) for the example case of Fig. 2 and Table 1. Interfacial forces on the source side $q_{iS}(t)$ $(i=1,2,3)$ and on the receiver side $q_{iR}(t)$ $(i=1,2,3)$ of all three paths are analyzed under two different input forces $f_S(t)$. First, an ideal impulse excitation is applied to observe the transient interfacial forces. Second, a periodic sawtooth excitation with period T=0.1 s and amplitude A=10 N as previously shown in Fig. 5(a) is selected; in this case, we add a significant Gaussian noise (with mean=0.5 N and variance=5 N^2) component to simulate the sensitivity of each method to random noise that is bound to be present in all real-life measurements. For each force input case, all initial conditions are assumed to be zero for the sake of convenience. To implement Method B, sampling parameters are selected as follows (refer to the prior discussion): f_{sp}=500 Hz with N_p=4096 (2^{12}) data points.

7.1. Ideal impulse force

The estimated path forces under an ideal impulse excitation are presented in Figs. 8 and 9 for paths 1 and 3, respectively, which correspond to the most and least dominant paths in terms of the transmitted forces. The results are given both in time and frequency domain for the first path in Fig. 8. The time domain methods (A–D) are compared in Figs. 8(b) and (d) from t=0 to1.0 s, and their frequency domain correspondents are given in Figs. 8(a) and (c), which correspond to the following four sets: (i) direct method in frequency domain as given by Eq. (1b); (ii) indirect method in frequency domain as expressed by Eq. (12) (Method B without taking the IFFT); (iii) FFT of the results yielded by Method C and (iv) FFT of the results yielded by Method D. Both time and frequency domain results show excellent consistency among the methods. In particular, Methods A,B,C are nearly coincident, and Method D shows only minor deviations. For path 3, only time domain results are presented (in Fig. 9) as we are primarily interested in the transient forces. Again, A,B and C virtually coincide, and Method D shows similar results though negligibly small deviations (compared with A, B or C) are seen especially at the peaks.

7.2. Comparison of interfacial forces for sawtooth force input with Gaussian noise

Next, a periodic sawtooth force input (with A=10 N and T=0.1 s) with a significant Gaussian noise (mean=0.5 N, variance=5 N^2) is applied at the source to observe the sensitivity of each method to the noise. No time domain averaging

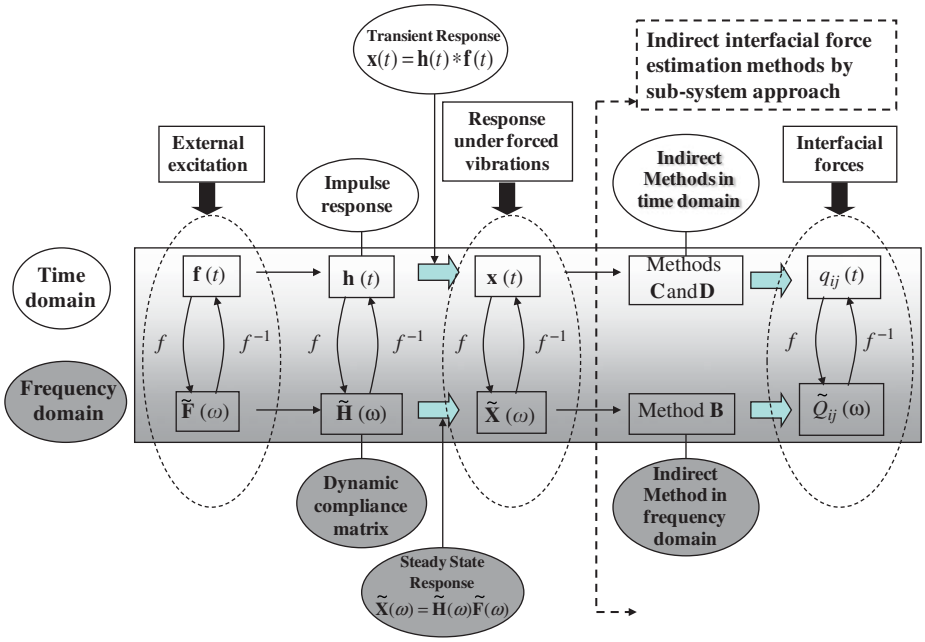

Fig. 7. Summary of time and frequency domain methods and the transformations. The right hand side of the dashed arrows show the indirect interfacial force estimation methods.

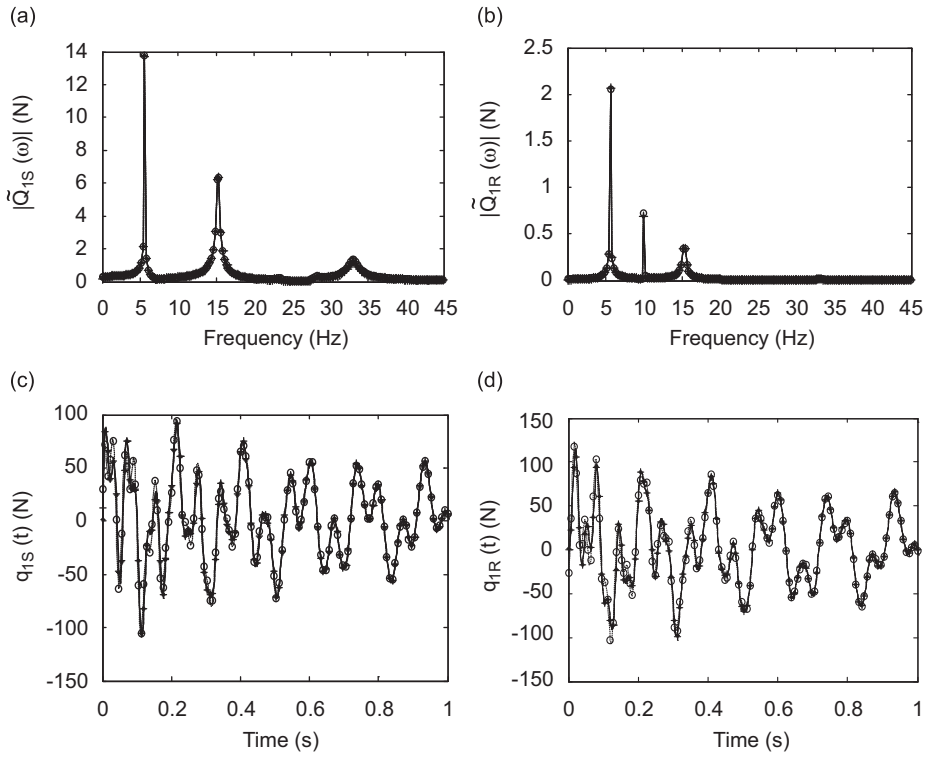

Fig. 8. Interfacial forces in path 1 when an ideal impulse force applied to the source: (a) $|\tilde{Q}_{1S}(\omega)|$; (b) $q_{1S}(t)$; (c) $|\tilde{Q}_{1R}(\omega)|$ and (d) $q_{1R}(t)$. Key (a), (c): (———), direct method in frequency domain by Eq. (1b); (◆◆◆◆◆), indirect method in frequency domain by Eq. (12) (Method B without IFFT); (+++++), FFT of Method C; (·o·o·o·o·o), FFT of Method D. Key (b),(d): (———), Method A; (◆◆◆◆◆), Method B; (+++++), Method C; (·o·o·o·o·o), Method D.

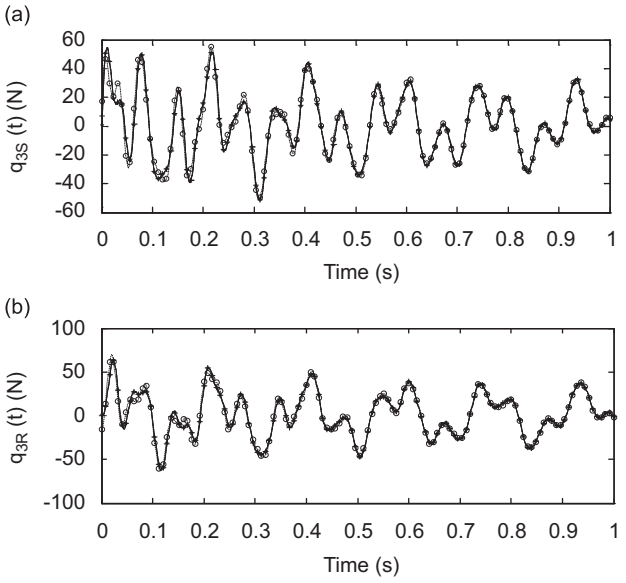

Fig. 9. Interfacial forces in path 3 when an ideal impulse force applied to the source: (a) $q_{3S}(t)$; (b) $q_{3R}(t)$. Key: (———), Method A; (◆◆◆◆◆), Method B; (+++++), Method C; (·o·o·o·o·o), Method D.

process (or any other noise reduction technique) is used. The results are shown in Figs. 10 and 11 for paths 1 and 3, respectively. The ideal interfacial forces (in the absence of noise) are also plotted for the time domain methods as the benchmark. Observe that all methods show some deviations, but it is difficult to tell which method (with noise) is closest

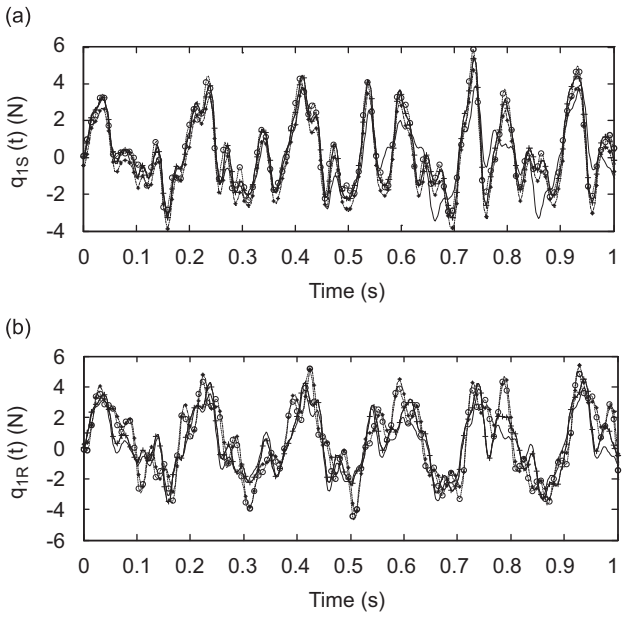

Fig. 10. Interfacial forces in path 1 when the noisy sawtooth force applied to the source: (a) $q_{1S}(t)$ and (b) $q_{1R}(t)$. Key: (———), Method A; (◆◆◆◆◆), Method B; (+++++), Method C; (·o·o·o·o·o), Method D; (———), ideal forces (without noise).

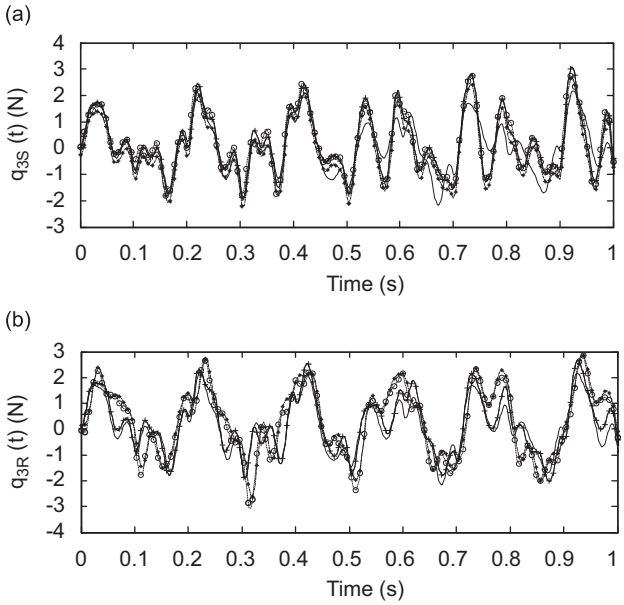

Fig. 11. Interfacial forces in path 3 when the noisy sawtooth force applied to the source: (a) $q_{3S}(t)$ and (b) $q_{3R}(t)$. Key: (———), Method A; (◆◆◆◆◆), Method B; (+++++), Method C; (·o·o·o·o·o), Method D; (———), ideal forces (without noise).

to the ideal (without noise). Methods A and C are almost coincident as they rely on the same calculated transient response. The deviations of Method D (not only from the ideal one but also from other curves) are even more visible especially for the interfacial forces on the receiver side.

To obtain more quantitative results, $\varepsilon_{\mathrm{rms}}$ (given by Eq. (17)) is calculated for each method based on time histories from t=0 to t=8.192 s ($=t_{\mathrm{sp}}$ for Method B). Here, $\varepsilon_{\mathrm{rms}}$ is also calculated with N_p=16,384 (2^{14}) data points for Method B (over the same time interval) in order to observe the effect of number of sampling points and the results are listed in Table 3. It may be seen that $\varepsilon_{\mathrm{rms}}$ for Method B with N_p=4096 (2^{12}) is very close to those of Methods A and C; such errors can be further reduced by selecting more sampling points. Method D has larger errors than other methods especially on the receiver side

(though still acceptable). Further analyses show that the mean of noise signal (and not the noise variance) controls most of the difference among the time domain methods. Overall, Method B seems to be slightly less sensitive to noise, but other time domain methods are still accurate and yield better results than Method B in certain time intervals. Thus, it would be a good practice to estimate the interfacial forces based on several methods rather than relying on a particular method especially in the presence high ambient (random) noise.

7.3. Method selection considerations

The feasibility studies clearly demonstrate that the time domain methods (A–D) yield (almost) an exact answer for an ideal input, and each one is capable of giving satisfactory results in the presence of random noise. However in practice, other considerations will dictate the choice of a method. For instance, Methods A and D essentially depend on the interfacial properties (i.e. k_{ij} and c_{ij}), which are usually difficult to estimate in many real-life problems. The applicability of Method C relies on the system modal parameters (when known). The accuracy of Method B, on the other hand, relies on the choice of sampling parameters as discussed before. Other signal processing issues such as leakage should also be considered when employing Method B. Thus, pure time domain methods (Methods A, C or D) are more desirable, when applicable, for transient conditions.

8. Preliminary experimental validation

To further validate the time domain methods, a simple experiment is developed and some initial results are obtained. Refer to Fig. 12(a) for the measurement setup, which consists of a plate–beam–plate structure to represent a source–path–receiver network, an impact hammer, an accelerometer and a two-channel FFT analyzer. The plate–beam–plate structure, which can be seen more clearly in Fig. 12(b), simulates the generic vibration problem well with parallel transmission paths as illustrated in Fig. 1; it consists of a source plate, a receiver plate, three parallel beams that act as transmission paths and finally compliant (rubber) materials as interfaces. These compliant materials, which reduce the number of modes of the overall system over the lower frequency regime, have low stiffness and high damping properties (though of unknown values) in comparison with those of the steel plates and beams. The source plate (m_S), the receiver plate (m_R) and the three identical parallel beams ($m_1 = m_2 = m_3$) are represented as pure mass elements with the following values: $m_S = 0.444$ kg, $m_S = 0.926$ kg and $m_1 = m_2 = m_3 = 0.08$ kg. Therefore it is convenient to model the system as a 5-DOF source–path–receiver network, just like in Fig. 2, with known **M** matrix but unknown **K** and **C** matrices.

An impulsive force $f_S(t)$ is applied to the source plate (m_S) with a force gauge equipped modal hammer, and the acceleration data of the paths in the vertical direction $\ddot{x}_i(t)$ ($i=1,2,3,R$) are measured by the accelerometer(s) and processed by the FFT analyzer, which also computes the accelerances $|\tilde{X}_i/F_S(\omega)|$ ($i=1,2,3,R$). The five resonance peaks ($\tilde{\mathbf{Q}}_r^{\text{peak}}$) of resulting spectra are estimated as the natural frequencies ($\hat{\Omega}_r$) of the 5-DOF model although only a few modes are dominant. Here, $\hat{}$ denotes an estimated value. The corresponding mode shapes are estimated as

$$\hat{\mathbf{u}}_r = \frac{\mathbf{u}_r^{\text{IP}}}{\sqrt{\mathbf{u}_r^{\text{IP}}\mathbf{M}\mathbf{u}_r^{\text{IP}}}} \quad \text{where } \mathbf{u}_r^{\text{IP}} = \text{Im}[\tilde{\mathbf{Q}}_r^{\text{peak}}] \tag{24}$$

The damping ratios ($\hat{\zeta}_r$) are estimated by the half-power method [29].

Since the system is a simple structure and one of the system matrices is already known (i.e. **M**), it is possible to estimate the structural properties (**K** and **C** matrices) of the system using the experimental data. If a good estimate of the system matrices can be found, it is easier to experimentally apply Method D rather than Method C. The structural properties (**K** and **C** matrices) can be estimated as

$$\hat{\mathbf{K}} = (\hat{\mathbf{U}}^{\text{T}})^{-1}\text{diag}[\Omega_r^2]\hat{\mathbf{U}}^{-1} \quad \text{and} \quad \hat{\mathbf{C}} = (\hat{\mathbf{U}}^{\text{T}})^{-1}\text{diag}[2\zeta_r\Omega_r]\hat{\mathbf{U}}^{-1} \tag{25}$$

Using these estimated system matrices, $\mathbf{x}(t)$ is determined by Eq. (3) from Eq. (4a), and $\dot{\mathbf{x}}(t)$ and $\ddot{\mathbf{x}}(t)$ are calculated using Eq. (5). A comparison of the measured and calculated accelerations $\ddot{x}_1(t) = (a_1(t))$ is shown in Fig. 13(a), which displays a

Table 3
Average root-mean-square errors (ε_{rms}) for each method when a noisy sawtooth force is applied to the source.

Method	ε_{rms} in interfacial force (N)					
	$q_{1S}(t)$	$q_{2S}(t)$	$q_{3S}(t)$	$q_{1R}(t)$	$q_{2R}(t)$	$q_{3R}(t)$
Method A	0.011	0.007	0.006	0.013	0.009	0.007
Method B, 4096 points	0.010	0.007	0.006	0.011	0.008	0.007
Method B, 16,384 points	0.006	0.004	0.004	0.008	0.006	0.004
Method C	0.011	0.007	0.006	0.013	0.009	0.007
Method D	0.012	0.008	0.006	0.017	0.013	0.011

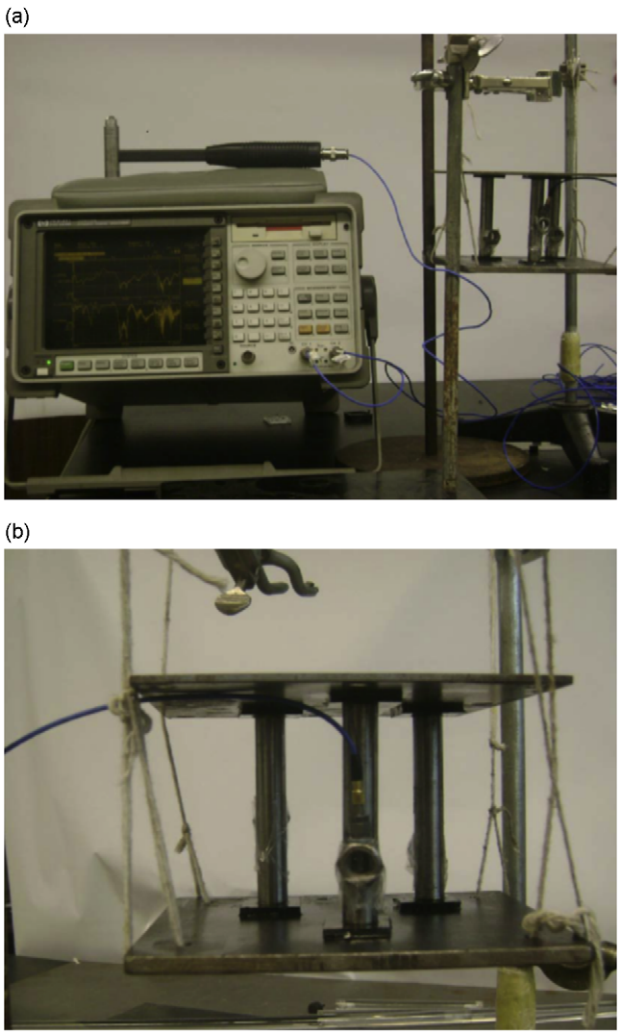

Fig. 12. Experimental configuration: (a) plate–beam–plate structure, impact hammer, accelerometer and a two-channel FFT analyzer and (b) a zoomed view to plate–beam–plate structure representing a source–path–receiver network. Compliant materials are inserted between the plates and the beams to represent the interfaces.

relatively good match. Knowing the $\mathbf{M}$, $\hat{\mathbf{C}}$ and $\hat{\mathbf{K}}$ matrices, $q_{iS}(t)(i=1,2,3)$ is now determined by Method D for both theoretical and experimental responses, and the resulting forces $q_{1S}(t)$ are shown in Fig. 13(b). The two curves show a consistent trend and the sources of error are the following: (i) integration of measured acceleration data; (ii) unwanted rigid body rotations and flexural motions of the source and receiver plates although an attempt is made to excite only the vertical motions; (iii) bias errors due to the lumped system model. The usage of a more continuous structure and an experimental application of sub-system approach might produce better results.

9. Conclusion

A structural path rank ordering process under transient excitations requires a good knowledge of the interfacial path forces, which are difficult to directly measure. Four time domain methods to estimate the interfacial forces are proposed and comparatively evaluated with application to linear time-invariant, proportionally damped discrete systems. First the transient response is outlined and a direct time domain technique (Method A) is given. Then the frequency domain estimation methods are reviewed, and the inverse Fourier transform scheme (Method B) is introduced. The transient interfacial forces are also derived from an alternate approach using the inverse modal analysis. The convolution integral assumes a summation form for discrete time data, and the trapezoid integration formula is inversely solved with regression algorithm about the generalized force $\mathbf{\Lambda}(t)$ in modal domain. The sub-system concept is employed to obtain the interfacial forces based on the forced vibration response of original system and modal data (Ω_r, ζ_r and $\mathbf{u}_r$) of the

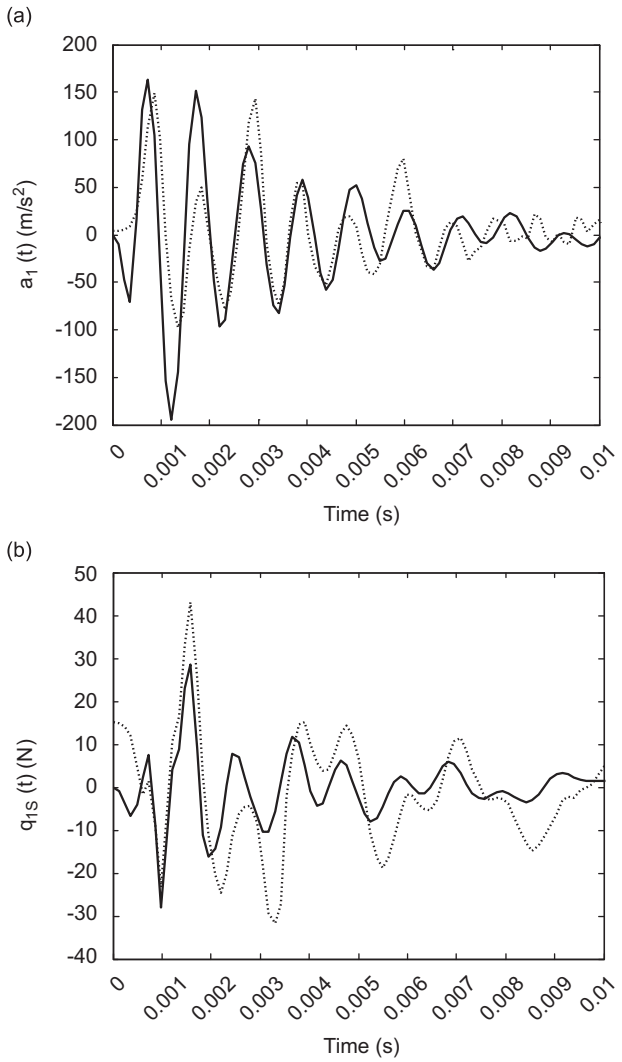

Fig. 13. Comparison of theoretical (———) and experimental (·····) results: (a) Acceleration on path 1 ($a_1(t)$) and (b) interfacial forces on the source side of path 1 ($q_{1S}(t)$).

sub-system (Method C). An approximate time domain scheme (Method D) is also suggested, which could be used only if the system properties are known or precisely estimated. The four interfacial force formulations are compared for a 5-DOF source–path–receiver system (with three parallel paths) under an ideal impulse and a noisy periodic sawtooth force. It is observed that Method C exactly matches Methods A and B though Method D also gives similar results with negligible deviations for an ideal impulse excitation. For a noisy periodic input some deviations are observed in each method although they are still satisfactory. Preliminary measurements on a laboratory experiment that utilizes Method D, are close to theoretical calculations though some deviations could be seen due to experimental sources of error.

The indirect formulations to estimate transient interfacial forces are novel time domain approaches. The proposed methods may overcome the errors introduced by the transfer function based frequency domain analyses (and related transformations) and may especially be useful to analyze lightly damped structures excited by transient excitations, or any particular system where the transient forces or responses are significant; this forms the key contribution of our article.

Acknowledgements

We are grateful to the member organizations of the Smart Vehicle Concepts Center (www.SmartVehicleCenter.org) and the National Science Foundation Industry/University Cooperative Research Centers program (www.nsf.gov/eng/iip/iucrc) for supporting this work.

Appendix A

A.1. Derivation of the convolution integral

The differential equations of motion of dimension N (Eq. (2)) may be solved using the Laplace (s) transformation $L[x(t)]=\bar{x}(s)$. Eq. (2) leads to $\bar{\mathbf{x}}(s)=\mathbf{Z}^{-1}(s)\bar{\mathbf{n}}(s)$, where dynamic stiffness is given by $\mathbf{Z}(s)=s^2\mathbf{M}+s\mathbf{C}+\mathbf{K}$. Dynamic force in the s domain is $\bar{\mathbf{n}}(s)=\bar{\mathbf{f}}(s)+(s\mathbf{M}+\mathbf{C})\mathbf{x}_0+\mathbf{M}B_0$, where $\mathbf{x}_0$ and $\dot{\mathbf{x}}_0$ are the initial displacement and velocity vectors, respectively. In order to execute the inverse Laplace transformation of $\bar{\mathbf{x}}(s)$, the characteristic equation $|\mathbf{Z}(s)|=0$, which results in a polynomial equation of order $2N$ in s, has to be numerically solved to obtain all poles of $\mathbf{Z}^{-1}(s)$. However, this approach becomes tedious with an increase in N, and thus the modal expansion approach must be adopted.

The time domain response $\mathbf{x}(t)$ can be expressed as a superposition of the normal modes for a proportionally damped system where $\mathbf{U}$ is the modal matrix. (The second number in parenthesis refers to the original equation number in the main paper):

$$\mathbf{x}(t)=\mathbf{U}\boldsymbol{\chi}(t) \quad \text{(A1) (3)}$$

Here, $\boldsymbol{\chi}(t)$ is the generalized coordinate (displacements). The external force in modal domain is also transformed as $\mathbf{U}^{\mathrm{T}}\mathbf{f}(t)=\boldsymbol{\Lambda}(t)$. By pre-multiplying Eq. (A1) with $\mathbf{U}^{\mathrm{T}}$ and taking advantage of orthogonal properties, the de-coupled equation of motion for the rth mode is as follows:

$$\ddot{\chi}_r+2\zeta_r\Omega_r\dot{\chi}_r+\Omega_r^2\chi_r=\Lambda_r, \quad r=1,2,\ldots,N \quad \text{(A2)}$$

The solution of Eq. (A2) can be obtained through the Laplace transformation:

$$\overline{\chi}_r(s)=\frac{\overline{\Lambda}_r(s)+(s+2\zeta_r\Omega_r)\chi_r(0)+\dot{\chi}_r(0)}{(s+\zeta_r\Omega_r)^2+\Omega_{rd}^2} \quad \text{(A3)}$$

where $\Omega_{rd}=\Omega_r\sqrt{1-\zeta_r^2}$; $\chi_r(0)$ and $\dot{\chi}_r(0)$ depend on the initial displacement and velocity, respectively, of the rth mode. Taking the inverse Laplace transformation of Eq. (A3), $\chi_r(t)=\chi_r^{\mathrm{CI}}(t)+\chi_r^{\mathrm{initial}}(t)$, where $\chi_r^{\mathrm{CI}}(t)$ is expressed by the convolution integral:

$$\chi_r(t)=\frac{1}{\Omega_{rd}}\int_0^t \Lambda_r(\tau)\mathrm{e}^{-\zeta_r\Omega_r(t-\tau)}\sin\{\Omega_{rd}(t-\tau)\}\,\mathrm{d}\tau+A_1(t)\chi_r(0)+A_2(t)\dot{\chi}_r(0) \quad \text{(A4a) (4a)}$$

$$A_1(t)=\mathrm{e}^{-\zeta_r\Omega_r t}\left(\cos\Omega_{rd}t+\frac{\zeta_r}{\sqrt{1-\zeta_r^2}}\sin\Omega_{rd}t\right); \quad A_2(t)=\frac{1}{\Omega_{rd}}\mathrm{e}^{-\zeta_r\Omega_r t}\sin\Omega_{rd}t \quad \text{(A4b-c) (4b-c)}$$

Then, the transient response is given by Eqs. (A1) and (A4).

A.2. Summation approximation of the convolution integral

For discrete time events including experimental data, the evaluation time is discretized at $t=t_1,t_2,\ldots,t_d(s)$ such that $t_1=0$ and time resolution $h=t_i-t_j$. At $t=t_2=h$, the integrand of χ_r^{CI} in Eq. (A4a) takes two values:

$$\tau=0: \ \Lambda_r(0)\mathrm{e}^{-\zeta_r\Omega_r h}\sin\Omega_{rd}h(\equiv I_1^{(0)}) \quad \text{(A5a)}$$

$$\tau=h: \ \Lambda_r(h)\mathrm{e}^{0}\sin 0=0 \quad \text{(A5b)}$$

Thus

$$\chi_r^{\mathrm{CI}}(h)=\frac{h}{2\Omega_{rd}}\Lambda_r(0)\mathrm{e}^{-\zeta_r\Omega_r h}\sin\Omega_{rd}h \quad \text{(A6)}$$

At $t=t_3=2h$, the integrand of χ_r^{CI} takes three values:

$$\tau=0: \ \Lambda_r(0)\mathrm{e}^{-2\zeta_r\Omega_r h}\sin 2\Omega_{rd}h\equiv I_2^{(0)} \quad \text{(A7a)}$$

$$\tau=h: \ \Lambda_r(h)\mathrm{e}^{-\zeta_r\Omega_r h}\sin\Omega_{rd}h\equiv I_2^{(h)} \quad \text{(A7b)}$$

$$\tau=2h: \ \Lambda_r(2h)\mathrm{e}^{0}\sin 0=0 \quad \text{(A7c)}$$

Thus

$$\chi_r^{\mathrm{CI}}(2h)=\frac{h}{\Omega_{rd}}I_2^{(h)}+\frac{h}{2\Omega_{rd}}I_2^{(0)} \quad \text{(A8)}$$

Next, at $t = t_4 = 3h$, the integrand of χ_r^{CI} takes four values:

$$\tau = 0: \ \Lambda_r(0)\mathrm{e}^{-3\zeta_r\Omega_r h}\sin 3\Omega_{rd}h \equiv I_3^{(0)} \tag{A9a}$$

$$\tau = h: \ \Lambda_r(h)\mathrm{e}^{-2\zeta_r\Omega_r h}\sin 2\Omega_{rd}h \equiv I_3^{(h)} \tag{A9b}$$

$$\tau = 2h: \ \Lambda_r(2h)\mathrm{e}^{-\zeta_r\Omega_r h}\sin \Omega_{rd}h = I_3^{(2h)} \tag{A9c}$$

$$\tau = 3h: \ \Lambda_r(3h)\mathrm{e}^{0}\sin 0 = 0 \tag{A9d}$$

Thus

$$\chi_r^{\mathrm{CI}}(3h) = \frac{h}{\Omega_{rd}}I_3^{(2h)} + \frac{h}{\Omega_{rd}}I_3^{(h)} + \frac{h}{2\Omega_{rd}}I_3^{(0)} \tag{A10}$$

Similarly, at $t = t_d = (d-1)h$, the convolution integral may be calculated by a sum of $(d-2)$ trapezoid areas and one triangle area as described below:

$$\tau = 0: \ \Lambda_r(0)\mathrm{e}^{-(d-1)\zeta_r\Omega_r h}\sin (d-1)\Omega_{rd}h \equiv I_{d-1}^{(0)} \tag{A11a) (6a}$$

$$\tau = h: \ \Lambda_r(h)\mathrm{e}^{-(d-2)\zeta_r\Omega_r h}\sin(d-2)\Omega_{rd}h \equiv I_{d-1}^{(h)} \tag{A11b) (6b}$$

$$\tau = 2h: \ \Lambda_r(2h)\mathrm{e}^{-(d-3)\zeta_r\Omega_r h}\sin(d-3)\Omega_{rd}h \equiv I_{d-1}^{(2h)} \tag{A11c) (6c}$$

$$\vdots$$

$$\tau = jh: \ \Lambda_r(jh)\mathrm{e}^{-(d-1-j)\zeta_r\Omega_r h}\sin(d-1-j)\Omega_{rd}h \equiv I_{d-1}^{(jh)} \tag{A11d) (6d}$$

$$\vdots$$

$$\tau = (d-1)h: \ \Lambda_r((d-1)h)\mathrm{e}^{0}\sin 0 = 0 \tag{A11e) (6e}$$

Therefore, the convolution integral in $\chi_r^{\mathrm{CI}}(t)$ is estimated by

$$\chi_r^{\mathrm{CI}}(t_d) = \chi_r((d-1)h) = \frac{h}{\Omega_{rd}}\sum_{j=1}^{d-2} I_{d-1}^{(jh)} + \frac{h}{2\Omega_{rd}}I_{d-1}^{(0)} \tag{A12) (7}$$

References

[1] A. Inoue, R. Singh, G.A. Fernandes, Absolute and relative path measures in a discrete system by using two analytical methods, *Journal of Sound and Vibration* 313 (2008) 696–722.

[2] J. Plunt, Strategy for transfer path analysis (TPA) applied to vibro-acoustic systems at medium and high frequencies, *Proceedings of ISMA* 23, Leuven, Belgium, September (1998) 16–18.

[3] C.V. Kurmaniak, C.V. Karsen, W.R. Kelley, Application of indirect force estimation techniques to the automotive transfer case, *Society of Automotive Engineers*, Paper # 1999-01-1764 (1999).

[4] A. Inoue, S. Kim, R. Singh, Comparative evaluation of structure-borne noise transfer paths in a laboratory experiment, *Noise Control Engineering Journal* 54 (6) (2006) 382–395.

[5] R. Singh, S. Kim, Examination of multi-dimensional vibration isolation measures and their correlation to sound radiation over a broad frequency range, *Journal of Sound and Vibration* 262 (3) (2003) 419–455.

[6] S. Kim, R. Singh, Multi-dimensional characterization of vibration isolators over a wide range of frequencies, *Journal of Sound and Vibration* 245 (2001) 877–913.

[7] J.D. Dickens, Direct force measurements of vibration isolators, *Noise Control Engineering Journal* 50 (5) (2002) 176–182.

[8] M.A. Gehringer, Application of experimental transfer path analysis and hybrid FRF-based substructuring model to SUV axle noise, *Society of Automotive Engineers*, Paper # 2005-01-1833 (2005).

[9] J.-H. Lee, K. Oh, Y.-S. Park, D.-H. Gwon, S.-K. Park, Transfer path analysis of structure-borne shock absorber noise in a passenger car, *Society of Automotive Engineers*, Paper # 2001-01-1441 (2001).

[10] Y. Wang, T.C. Lim, M.L. Clapper, N.-M. Shiau, P. Braunwart, Y. Lee, Driveline NVH modeling applying a multi-subsystem spectral-based substructuring approach, *Society of Automotive Engineers*, Paper # 2005-01-2300 (2005).

[11] Y. Kanda, T. Saka, M. Fujikawa, K. Ando, I. Sako, I. Kawahara, Experimental transfer path analysis of gear whine, *Society of Automotive Engineers*, Paper # 2005-01-2288 (2005).

[12] F. Haste, A. Nachimutu, Calculating partial contribution using component sensitivity values: a different approach to transfer path analysis, *Society of Automotive Engineers*, Paper # 1999-01-1693 (1999).

[13] J.R. Blough, A survey of DSP methods for rotating machinery analysis, what is needed, what is available, *Journal of Sound and Vibration* 262 (2003) 707–720.

[14] S.R. Ibrahim, E.C. Mikulcik, The experimental determination of vibration parameters from time responses, *The Shock and Vibration Bulletin* 46 (1976) 187–196.

[15] S.R. Ibrahim, E.C. Mikulcik, A method for the direct identification of vibration parameters from the free response, *The Shock and Vibration Bulletin* 47 (1977) 183–198.

[16] S.F. Masri, R.K. Miller, A.F. Saud, T.K. Caughey, Identification of nonlinear vibrating structures: part I–—formulation, *Transactions of the ASME* 54 (1987) 918–922.

[17] M. Haroon, D.E. Adams, Y.W. Luk, A technique for estimating linear parameters using nonlinear restoring force extraction in the absence of an input measurement, *Journal of Vibration and Acoustics* 127 (2005) 483–492.
[18] X.Y. Li, S.S. Law, Identification of structural damping in time domain, *Journal of Sound and Vibration* 328 (2009) 71–84.
[19] J.S. Kang, S.K. Park, S.B. Shin, H.S. Lee, Structural system identification in time domain using measured acceleration, *Journal of Sound and Vibration* 288 (1–2) (2005) 215–234.
[20] S.B. Shin, S.H. Oh, Damage assessment of shear buildings by synchronous estimation of stiffness and damping using measured acceleration, *Smart Structures and Systems* 3 (3) (2007) 245–261.
[21] A.N. Thite, D.J. Thompson, The quantification of structure-borne transmission paths by inverse methods, part 2: use of regulation techniques, *Journal of Sound and Vibration* 264 (2003) 433–451.
[22] H.R. Busby, D.M. Trujillo, Optimal regularization of an inverse dynamics problem, *Computers and Structures* 63 (2) (1997) 243–248.
[23] Y. Liu, W.S. Shepard Jr., Dynamic force identification based on enhanced least squares and total least-squares schemes in the frequency domain, *Journal of Sound and Vibration* 282 (2005) 37–60.
[24] E. Jacquelin, A. Bennani, P. Hamelin, Force reconstruction: analysis and regularization of a deconvolution problem, *Journal of Sound and Vibration* 265 (2003) 81–107.
[25] Q. Leclere, C. Pezerat, B. Laulagnet, L. Polac, Indirect measurement of main bearing loads in an operating diesel engine, *Journal of Sound and Vibration* 286 (2005) 341–361.
[26] T.G. Carne, V.I. Bateman, R.L. Mayes, Force reconstruction using a sum of weighted accelerations technique, *Proceedings of the 10th International Modal Analysis Conference* (1992) 291–298.
[27] A.D. Steltzner, D.C. Kammer, Input force estimation using an inverse structural filter, *Proceedings of IMAC* 17 (1999) 954–960.
[28] T. Lim, W. Pilkey, A solution to the inverse dynamics problem for lightly damped flexible structures using a modal approach, *Computers and Structures* 43 (1) (1992) 53–59.
[29] L. Meirovitch, *Fundamentals of Vibrations*, McGraw Hill, New York, 2001.
[30] N.M.M. Maia, J.M.M. Silva, editors in chief, *Theoretical and Experimental Modal Analysis*, Research Studies Press, Somerset, England, 1997.
[31] P. Gardonio, S.J. Elliott, R.J. Pinnington, Active isolation of structural vibration on a multiple-degree-of-freedom system, part I: the dynamics of the system, *Journal of Sound and Vibration* 207 (1) (1997) 61–93.
[32] P. Gardonio, S.J. Elliott, Passive and active isolation of structural vibration transmission between two plates connected by a set of mounts, *Journal of Sound and Vibration* 237 (2000) 483–511.
[33] O. Guasch, Direct transfer functions and path blocking in a discrete mechanical system, *Journal of Sound and Vibration* 321 (2009) 854–874.
[34] F.X. Magrans, Method of measuring transmission paths, *Journal of Sound and Vibration* 276 (2004) 335–359.
[35] J.S. Bendat, A.G. Piersol, *Random Data: Analysis and Measurement Procedures*, second ed., Wiley-Interscience, New York, 1986.